Urban Climate

Volume , Part , October 2016, Pages

Predicting Surface Temperature Variation in Urban Settings Using Real- Time Weather Forecasts

Predicting Surface Temperature Variation in Urban Settings Using Real-Time Weather Forecasts

Maryam Karimi[a,b], Brian Vant-Hull[c], Rouzbeh Nazari[d*], Megan Mittenzwei[d] and Reza Khanbilvardi[c]

[a]*Columbia University Mailman School of Public Health, 722 W 168th Street, New York, 10032, United states*
[b]*The Graduate Center, the City University of New York, 365 5th Avenue, New York, 10016, United States*
[c]*NOAA Crest, City College of New York, 160 Convent Avenue, New York, 10031, United States*
[d]*Department of Civil and Environmental Engineering, Rowan University, 211 Mullica Hill Rd, Glassboro, New Jersey, 08028, United States*

Abstract

Densely populated cities experience adverse effects of Urban Heat Island (UHI) including higher numbers of emergency hospital admissions and heat related illnesses. Studying UHI effects and temperature variations has become even more important as global temperatures continue to rise. To better understand UHIs within New York City, an exploratory study was done using a field campaign to measure high resolution spatial and temporal temperature variations within Manhattan's urban setting. These time correlated temperature measurements along with weather model data of temperature and relative humidity were used to predict temperature variability using weather forecasts. The amplitude of spatial variations was most dependent on temperature (r = 0.400) and low level lapse rate (r = -0.258) while temporal variations were most dependent on temperature (r = 0.398), low level lapse rates (r = -0.361), and mid-level lapse rate (r = -0.320). Regression of weather variables can be used to predict the amplitude of spatial and temporal variation in temperature within a city for each day. This study directs attention towards high resolution near-surface air temperature analysis and offers a new look at surface thermal properties. The application of the resulting data and modeling is most suitable for forecasting microscale variability in urban settings.

Keywords: *Surface Temperature Variation, Weather Forecast, High Resolution Data, Urban Heat Island, Human Health*

*Corresponding Author. Tel: +0-856-256-5352, fax: +0-856-256-5242.
E-mail address: nazari@rowan.edu

1. Introduction

UHI effects or local hotspots are common phenomenon experienced in urban settings. These concentrated areas of elevated temperature "represent one of the most significant human–induced changes to Earth's surface climate" (Zhao et al., 2014). UHI is caused by lack of evapotranspiration, waste heat produced by air conditioning, industries and vehicles, air pollution and radiative trapping due to land surface modification in cities (Oke, 1982). The above factors lead to increase in air and surface temperature in urban centers and convection of heat from surface temperatures into the lower atmosphere. Local climate can impact UHI and alter convection patterns, and so statistical models of local climate/weather may help create forecast models for predicating temperature variations at surface level (Zhao et al., 2014). A number of heat transfer mechanisms that vary throughout a city can cause variations in air temperature. For instance, absorption of sunlight will vary by albedo and shading due to building materials and geometry. Infrared radiation is absorbed and re-radiated by surrounding structures, so that variations in exposure to the sky (sky view fraction) will cause variations in radiation cooling. These factors affect surface temperature, which is transferred to the air depending on wind flow. More exposed areas will have both more radiation cooling as well as faster wind flow, so that the heat transfer per volume of air is less, leading to cooler air temperatures. Note that weather variables may have dual effects: higher wind may result in greater air temperature contrasts between exposed and sheltered areas while mixing air between areas. Full cloud cover will produce less variation due to solar heating, and also less variation due to infrared cooling. In studying UHI effects understanding inner city temperature variations are important because health impacts are a sensitive function of temperature (Kinney et al., 2008), so temperature variability within a densely populated area can have large effects.

The U.S. EPA Climate Change Indicators report released its extreme heat section statement of May 2014 specifying that "the number of increased heat-related deaths in the future is going to be greater than the number of reduced cold-related deaths" (2014). "Heat is the number one weather-related killer in the U.S. alone" (EPA, 2014). Profound impacts of UHI are seen on the lives of those who reside in cities (Zhao, 2014). Hotter days are associated with serious health impacts, heart attacks and respiratory and cardiovascular diseases (Kenward et al., 2014). Extreme climate events are predicted to increase in number, duration, and frequency with on-going climate change (Astrom et al., 2011). In recent decades, several devastating heat waves have caused large health consequences across the globe. For example, the 1987 heat wave caused around 2000 deaths in Athens; the 1995 Chicago heat wave caused around 700 deaths; and the 2003 heat wave in Europe was estimated to have caused 70 000 deaths (Katsouyanni et al., 1988; Semenza et al., 1996).

Densely populated cities like Manhattan can be affected by the impact of UHI much more than less populated cities. Urbanization increases "the diurnal minima and the daily means in all seasons" (Karl et al., 1988). Manhattan lacks evaporative cooling from vegetation and moist soil, and retains heat with its buildings and pavements which causes radiative trapping in canyons. The typical physical features of Manhattan's land surface and its mixture of land cover reacts differently with UHI, causing smaller islands of urban heat throughout the city (Grimmond, 2007). As the impact of UHI increases so does the health risks of heat wave. Even though many studies have been focused on the impact of UHI and temperature changes between urban and rural air temperature, not many look at the temperature variations within a city. These studies mostly use remote sensing data such as MODIS, Landsat and Aster or typical measurements collected by local meteorological station networks. High resolution satellites suitable for urban studies are polar orbiting and tend to be sun synchronous, so do not capture diurnal variations; while the highest resolution instruments such as Landsat have narrow swaths and repeat times on the order of weeks. Cloud free conditions are required. Moreover, satellites measure surface temperatures including rooftops and treetops rather than air temperature. For these reasons a set of surface instruments is preferable for capturing weather effects on urban temperature variability.

In local meteorological study, mobile traverses measured temperature variations within in a town in Hungary four hours after the sunset to find the impact of UHI. In regression of its measured temperature against building fraction, water fraction, and sky view fraction correlations of 0.8 to 0.9 were calculated based on the season. Ho et al. (2014) used 60 weather stations in the Vancouver area to develop a model for air temperature given sky view fraction, vegetation, elevation and solar radiation. Comrie (2000) mapped the heat island of Tucson Arizona using mobile instruments, and attributed most inner city temperature variability to cool air drainage from the mountains. Eliasson (1996) was able to predict the differences in temperature between two urban locations (open and urban canyon) based on regression of weather variables. A study using a combination of mobile and

fixed instruments in Granada mapped the structure of the heat island and noted how the amplitude decreased with wind speed and cloudiness (Montavez et al., 2000).

Whereas previous mentioned studies of the evaluation of UHI variability have only focused on urban and rural air temperature, the current study will uniquely look at spatial and temporal variation in temperature within a city using weather forecast model run by the National centers for Environmental Prediction (NCEP). The weather forecast model from NCEP generates multiple grids of weather forecast over North America for different horizontal resolutions using numerical weather models. The final product of this work will lead to a statistical model that could predict air temperature and variability within a city based on weather factors. At this stage the analysis should be considered exploratory.

2. Methodology

HOBO Micro-Station Data Loggers (Onset Product #: H21-002) which consist of relative humidity and temperature sensors were installed inside white instrument shelter boxes and mounted 3-4 meters above ground on lampposts at ten different stations throughout the island of Manhattan. Data was taken, starting June 23, 2013, in three minute intervals for the entire period of the study, ending September 20, 2013. Figure 1 shows the locations of the ten stations (a), sensors (b), and the equipment mounted on a lamppost (c).

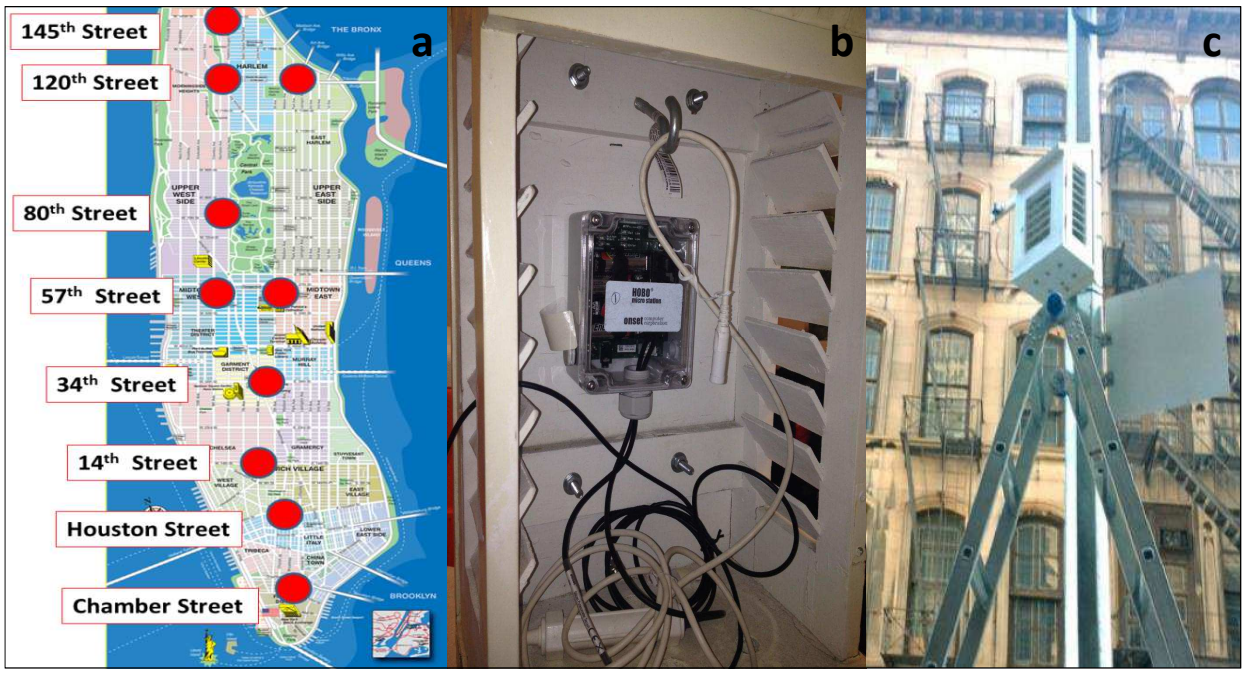

Fig 1. Station Locations (red circles indicate the location of the stations), Instrument and Instrument Housing

The locations of the shelters were picked based on street routes from a previous study "with locations selected to capture the range of variability noted in the walking campaigns of 2012" (Vant-Hull et al., 2014). The first station located at 63A Reade Street (South side of the street), the second located at 118 Prince Street (North side), the third station located at 140 E. 14th Street (South side), the fourth located at 146 E. 35th Street (South side), the fifth located at 114 E. 57th Street (South side), the sixth located at 348 W. 57th Street (South side), the seventh located at 211 Central Park West (East side), the eighth located at 346 E. 120th Street (South side), the ninth located at 150 W. 120th Street (South side), and the tenth located at 300 W 145th Street (South side). Further information regarding descriptions of the areas of which each station was located is available in Table 1.

Table 1. Physical Description of Areas Surrounding Stations

Station #	Street Description	Latitude (N)	Longitude (W)	MSL (m)	AGL (m)	B-Avg. Fraction	B-Avg. Height (m)	Sky View	NDVI* Avg.
1	17 m wide, no trees	40.71497	74.00659	9	3.7	0.94	46	0.06	0.12
2	13.5 m wide, no trees	40.72513	73.99974	7	3.4	0.74	28	0.28	0.11
3	27 m wide, few trees	40.73353	73.98815	11	3.9	0.65	42	0.35	0.05
4	18 m wide, some trees	40.74618	73.97871	14	3.1	0.66	40	0.34	0.02
5	33 m wide, some trees	40.76123	73.96993	14	3.4	0.59	71	0.41	0.20
6	32 m wide, many trees	40.76747	73.98488	25	3.5	0.57	70	0.42	0.13
7	15 m wide, in trees	40.78233	73.97137	30	3.3	0.66	51	0.34	0.25
8	31 m wide, many trees	40.79877	73.93413	3	3.5	0.10	4	0.96	0.04
9	21 m wide, many trees	40.80534	73.94968	8	3.1	0.70	25	0.33	0.34
10	28.5 m wide, some trees	40.82298	73.94274	9	3.3	0.63	22	0.40	0.20

Mean Sea Level (MSL) describes the instruments' height above sea level, Above Ground Level (AGL) describes the instruments' height above ground level

In the table above: (description of each category) the street description provides the street width along with the tree coverage ("no trees" = temperature will be unaffected, "few trees" = tree coverage unlikely to affect temperature, "some trees" = may affect temperature if wind blowing through, "many trees" = wind will always blow through and instrument has some sky fraction, "in trees" = no sky view through the trees), , the building average fraction (B-Avg. Fraction) indicates the fraction of buildings in the zip code that each station is located in, the "B-Avg. Height" is the average height of buildings in meters in the zip code that each station is located in, Sky view fraction is the amount of direct sky above the instrument estimated from the building parameters.

The sky view fraction is estimated from the building parameters and was calculated using the method of Gladt and Bednar (2013). Normalized Difference Vegetation Index- is a graphical indicator used to analyze remote sensing measurements for green vegetation. NDVI is calculated from the red and Near-Infrared Radiation (NIR) bands as the ratio of (NIR-RED) to (NIR+RED), so that it varies between -1 to +1 (Zhang et al., 2006; Voogt et al., 2003). To accommodate adjacency effects the average values from 3x3 LandSat pixels centered on each instrument is used. Vegetation yields high NDVI, soil registers near zero, and clouds and water produce negative NDVI values. The zero vegetation offset is near NDVI = 0.1, but as it can vary with background no offset was applied.

This study focused on midafternoon temperatures at 1500 Local Time (LT) and considered the spatial and temporal variabilities that were assumed to affect weather predictions. Days with rainfall within an hour of this time were dropped from the data set. The spatial variability in temperature is assumed to be due to differences in surface features alone. The temporal variability represents local changes in temperature caused by convection and perhaps mechanical turbulence plus temporal variability of large scale weather patterns. The related field campaigns with portable instruments recorded spatial variability across all axes which were attributed mainly to changes in elevation

and vegetation (Karimi et al., 2015). Any regional gradient in temperature is not immediately apparent on this scale (10 km).

Manhattan is small compared to large-scale weather patterns, so we assume all instruments are exposed to the same weather variables. The diurnal patterns of variability in temperature were reported in Vant-Hull et al. (2014). These large, slower changes in temperature were filtered out of the calculation of temporal variability by use of a running average to define fluctuations in temperature. An exploration of diurnal changes in urban temperature variability will be left for a future study.

In processing the campaign datasets, the spatial temperature standard deviation (σ_S) was calculated in two steps. At each location the data over the course of an hour was averaged to eliminate the convection variation. The standard deviation of all 10 stations' hourly averages was then calculated to get σ_S. The temporal variation for each hour was also calculated in two steps. First the one-hour running average temperatures at each location were subtracted from the local temperatures to find the temperature fluctuations from the average for each 3 minute interval. These fluctuations over a one hour period were used to calculate the temporal standard deviation (σ_T).

Weather variables that relate to the amplitude of fine scale temperature anomalies include temperature (T ^oC), relative humidity (RH%), Eastward wind speed (v), Northward wind speed (u), and lapse rate (LR) from the North American Model Reanalysis data set archived by the National climatic Data Center (available every three hours with a 40 km resolution and a vertical resolution of 25 millibar near the surface (roughly 250 meters)). Low-Level Lapse Rate (LR) is the slope of change in temperature with height (dT/dH) at atmospheric pressures between 975 and 950 millibar grams (mb) and temperature differences between 975 and 950 mb, and was calculated as degrees C per km. Other variables affecting temperature include cloud fraction (CF), wind speed (WS), which is the vector magnitude of u and v, and evaporation rate (ER) calculated as (WS)(1-RH/100). ER does not include soil moisture or other transpiration factors such as light.

The variability in T, σ_S and σ_T, were regressed against weather variables to determine their effects on spatial and temporal variability in urban temperatures.

$$(\text{Temperature variability } \sigma_S \text{ or } \sigma_T) = c_0 + c_1X_1 + c_2X_2 \ \ldots + c_nX_n \qquad (1)$$

where $\sigma_{S,T}$ are vectors of temperature variability through time (one value per day),
X_i are the associated weather variable vectors (n variables, one value per day),
c_i are linear coefficients found by regression (n+1 constants).

Single variable correlations between each weather variable and the spatial or temporal temperature variabilities were also calculated. These statistical quantities appear in tables 2 and 3 for spatial and temporal temperature variability, with similar calculations in table 4 (explained below).

3. Results and Discussion

The result of calculated correlation between the spatial temperature variability σ_S and weather variables show the highest correspondence with T (r = 0.40) followed by LRlow (r = -0.26). Components of wind are next in significance, after which correlations drop down to 0.1 or lower. However all physically meaningful variables are included in the regression despite low single variable correlations due to the possibility of statistical suppression effects (MacKinnon et al., 2000), whereby cross-correlations may mask significant relationships. The results of the correlation between σ_S and the weather variables can be seen in Table 2.

Table 2. Correlation between observed σ_S and weather model variables. All variables are defined in text

Variable	Coefficient	Correlation (r)	Variance(r^2)
T (C)	0.014	0.400	0.160
RH (%)	0.002 C	- 0.160	0.027
V (m/s)	-0.017 Cs/m	- 0.170	0.027
U (m/s)	0.000 Cs/m	0.150	0.021
WS (m/s)	- 0.009 Cs/m	- 0.038	0.001
ER (m/s)	0.024 Cs/m	0.069	0.004
LR (C/km)	- 0.011 km	- 0.260	0.067
CF (%)	0.000 C	0.110	0.012

The results of the correlation between σ_T and the weather variables can be seen in Table 3.

Table 3.Correlation between observed σ_T and weather model variables. All variables are defined in text

Variable	Coefficient	Correlation (r)	Variance (r^2)
T (C)	0.003	0.400	0.160
RH (%)	- 0.000 C	- 0.310	0.095
V (m/s)	0.004 Cs/m	0.150	0.024
U (m/s)	- 0.001 Cs/m	0.019	0.000
WS (m/s)	0.001 Cs/m	- 0.120	0.014
ER (m/s)	- 0.003 Cs/m	- 0.031	0.001
LR (C/km)	- 0.0028 km	- 0.360	0.130
CF (%)	-0.000 C	- 0.120	0.014

From the weather variables in table 3; T, LR and RH show the highest correlations to temporal variability in temperature. Given the complexity of the mechanisms involved, the discussion of physical effects in the following two paragraphs is intended to stimulate further investigation, and does not represent conclusions derived from the data.

Spatial variability in mid-day temperature has the strongest correlation to temperature itself (Table 2), which may be related to warmer days having clear skies and greater differential solar heating among surface features. The vertical atmospheric temperature lapse rate (LR) can affect surface temperature variability through topographical variability (Table 2). But this is insufficient, for we have noted in previous work in Manhattan that variations with air temperature near the surface often change faster with elevation than the atmospheric lapse rate (Karimi et al., 2015). The winds are next in order of significance, and can have competing effects on spatial temperature variability. Wind could smooth out surface variations through mixing, or it may cause air to flow faster over elevated, exposed surfaces while air in sheltered low areas will have more time to absorb heat from sunlight surfaces. The regression coefficients of Table 2 exhibit such competing effects on the spatial temperature variability based on wind direction, which may be related to topography and sea-breeze; but the statistics are not strong enough to allow further speculation on this rather complex situation.

Temporal variability in temperature was measured on the scale of minutes, capturing convective and turbulent time scales. Since spatial temperature variability increases with temperature (Table 2), these spatial fluctuations will be converted to temporal fluctuations at any given location via turbulent transport, providing the correlation to temperature seen in Table 3. Convective mixing at the surface is strongly coupled to the low-level lapse rate, so more negative lapse rates should result in greater temporal variability in temperature as seen in Table 3. It is not clear why RH has a strong negative effect on temporal temperature variability. It would seem higher RH would stimulate clouds and convection with higher variability, but the effect is opposite of the expected. It is possible that higher RH results in lower evaporative cooling, but it is not reflected in the evaporation rate term.

To visually clarify the patterns between the weather variables and spatial and temporal variability, the regressed relationships were graphed (Figs 2 and 3) versus the observations of temperature variability.

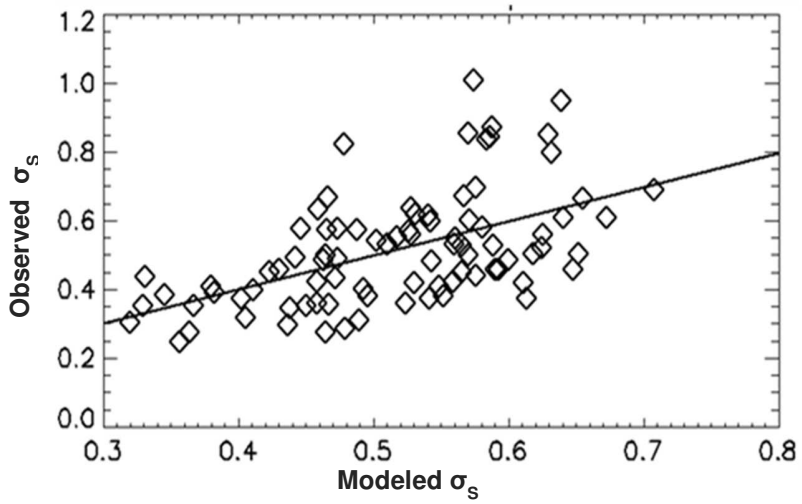

Fig 2. Weather model variables vs. observed σ_S values, where each data points represents an average hourly value.

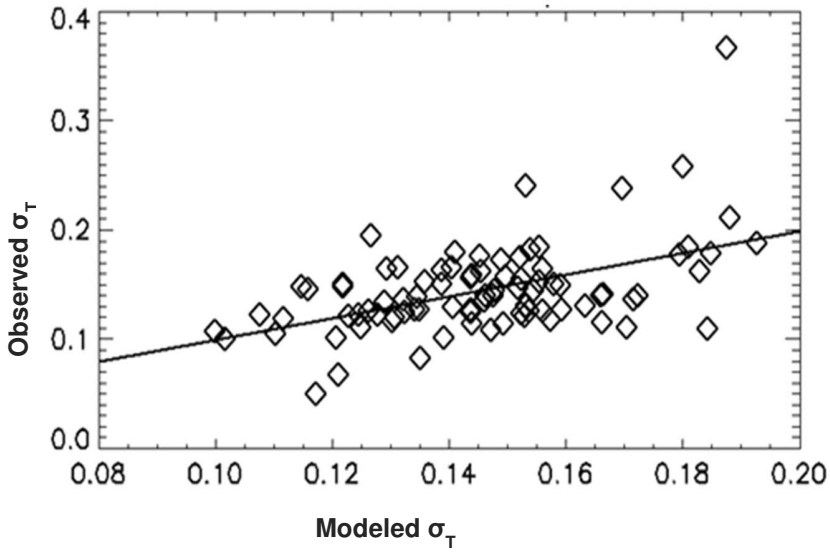

Fig 3. Weather model variables vs. observed σ_T, where each data points represents one-hour running average.

In fig 2and 3, each point represents the σ of observed temperature values vs. modeled values from eq. (1) for each day in the 3 month experiment. The multiple-variable regression coefficients for σ_S and σ_T were calculated as 0.541 and 0.501 and can be seen in the graphs as the range of predictability that the statistical model can have for a given weather conditions. It is also noted that the spatial variability at a level of three or four meters above the ground is as much as ¼ the variability at a typical human trunk height of one and half meters (Vant-Hull et al., 2014), due to the steep temperature gradient in air temperature near the surface. The temperature variations shown in the plots above therefore underestimate the temperature variability seen by pedestrians. This shows that temperature variability estimated from weather forecasts exhibit moderate skill in predicting spatial and temporal temperature variability within cities.

To further examine the role of topography in temperature variability, the relationships of weather variables to the temperature difference between stations at high and low elevation were calculated (table 4). This was done to study the impact of winds on the variation of temperature between the lowest (57St West) and highest (120St West) streets stations. The trend line in fig 4 shows a moderate multi-variable correlation of 0.5 between weather variables and temperature difference.

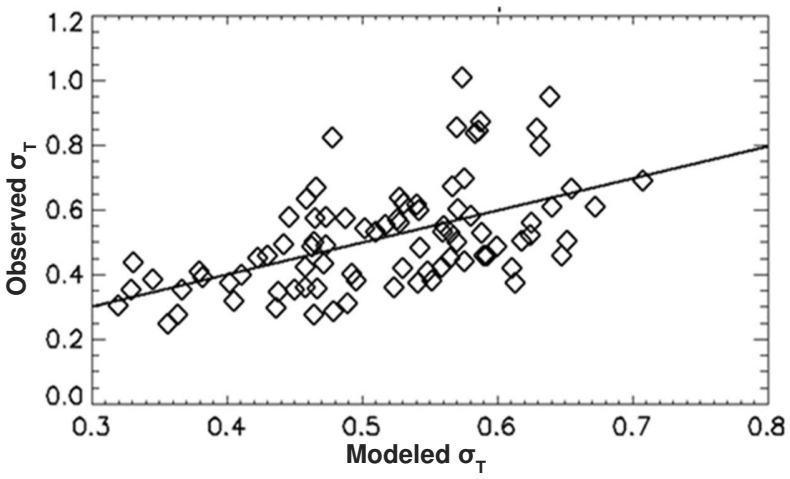

Fig 4. Weather model variables vs. observed σ_T for the highest and lowest elevation stations. Each data point represents an average hourly value.

Table 4. Correlation between high and low elevation station temperature differences and weather model variables. All weather variables are defined in text

Variable	Coefficient	Correlation (r)	Variance (r^2)
T (C)	0.067	0.470	0.220
RH (%)	0.011 C	- 0.130	0.018
V (m/s)	0.012 Cs/m	0.190	0.035
U (m/s)	0.025 Cs/m	0.280	0.077
WS (m/s)	- 0.001 Cs/m	0.018	0.0003
ER (m/s)	0.024 Cs/m	0.076	0.006
LR (C/km)	- 0.042 km	- 0.216	0.047
CF (%)	- 0.003 C	- 0.047	0.002

Table 4 shows a clear correlation between the average temperature and the temperature difference between the two stations. U, the component of wind most nearly perpendicular to the ridge that runs along Manhattan, shows a larger correlation to the temperature difference than the nearly parallel component V. This directionality may explain why there is such a low correlation to the total wind speed WS. As expected the lapse rate is among the top three variables correlated to temperature differences with elevation.

Regional weather patterns such as sea breeze can set up temperature gradients that might affect the spatial temperature variability, producing a false signal that is not due to more highly localized urban or elevation effects. To examine this we turn to the NYC MetNet of the Optical Remote Sensing Laboratory of the City University of New York, which includes a network of volunteer weather stations throughout the New York metropolitan area (Meir et al., 2013). Figure 5 shows a typical low-wind day (a), an average of all low-wind days of the summer of 2013 (b), and averages of all day with winds from the NNW quadrant or winds from the SSE quadrant (c and d), since these were the predominant wind directions. To capture temperature patterns without being dominated by extreme days, the data was centered about the average each day and normalized by the standard deviation.

The low-wind sample day (a) shows a clear sea breeze pattern, with a gradient perpendicular to Manhattan's axis. Since the sensors used in this work were largely aligned along the axis of Manhattan (Fig 1) the effects of this gradient are minimized. When all low wind days are averaged (b) the pattern largely vanishes, perhaps due to cloudy days that do not exhibit sea breeze. The average of all days with wind from the NW (c) exhibits a near reversal of the sea breeze pattern, so the gradient effect is again minimized. Rather surprisingly the average of all SW days appears to show a reversed sea breeze pattern as well. In summary the regional gradients are largely (but not completely) mitigated by placing the sensors perpendicular to the predominant direction of the gradients.

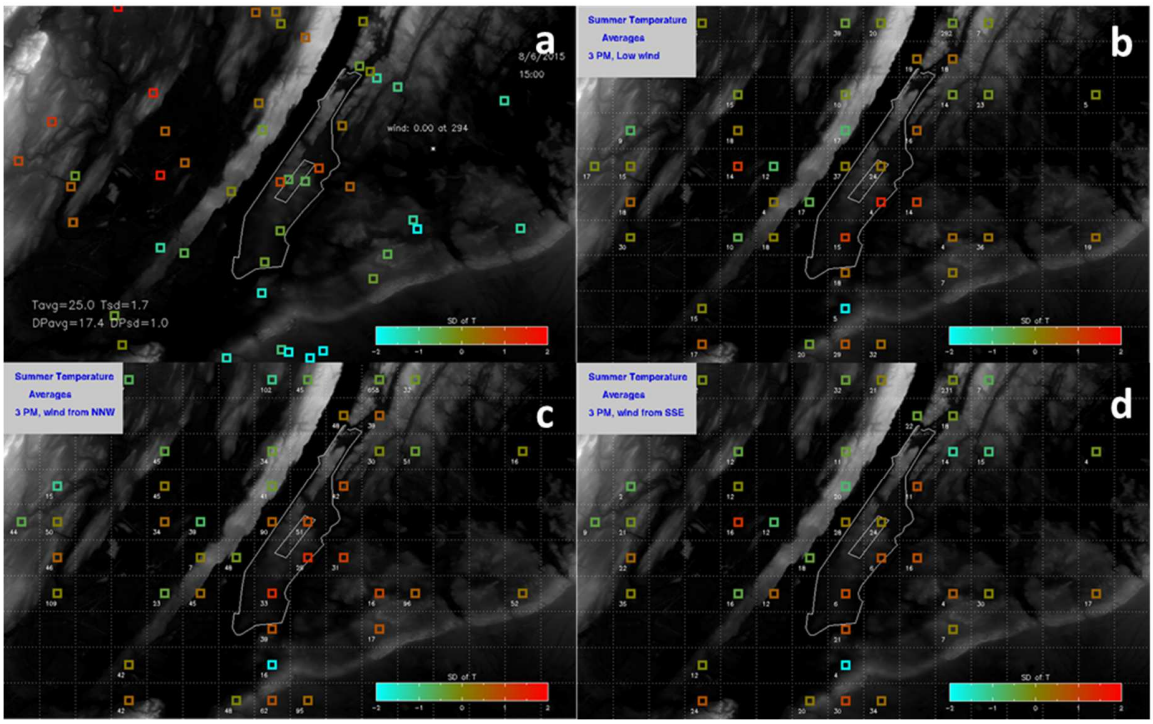

Fig 5. NYC MetNet Average Normalized Temperatures Compared to Single Day. Blue (-2 to -1), green (-1 to 0), orange (0 to 1), and red (1 to 2). (a) shows a single day with no wind and a clear temperature gradient, (b) shows Summer temperature averages with no wind, (c) shows Summer temperature averages with wind coming from the North-Northwest direction, and (d) shows Summer temperature averages with wind coming from the South-Southeast direction.

4. Conclusion

There are a number of heat transfer mechanisms that will vary throughout a city, causing variations in air temperature. Absorption of sunlight will vary by albedo and shading due to building materials and geometry. Infrared radiation is absorbed and re-radiated by surrounding structures, so that variations in exposure to the sky (sky view fraction) will cause variations in radiation cooling. These factors affect surface temperature, which is transferred to the air depending on wind flow. More exposed areas will have both more radiation cooling as well as faster wind flow, so that the heat transfer per volume of air is less, leading to cooler air temperatures. Note that weather variables may have dual effects: higher wind may result in greater air temperature contrasts between exposed and sheltered areas while mixing air between areas. Cloud cover will produce less variation due to solar heating, yet less variation due to infrared cooling. The regressed relationships between weather variables and the spatial and temporal temperature variabilities can be used to predict variability under given conditions.

This exploratory study helps to understand the urban heat island effect within Manhattan using field campaign temperature measurements. The high resolution temporal and spatial temperature measurements were correlated with weather model data to predict temperature variability. The amplitude of spatial variations of temperature was most dependent on average temperature ($r = 0.40$) and temperature lapse rate ($r = -0.26$) while temporal variations were most dependent on average temperature ($r = 0.4$), relative humidity ($r = -0.31$), and temperature lapse rate ($r = -0.36$). Winds can increase spatial variations in temperature, and our evidence links this to elevation differences. Lapse rates have a large effect on the temporal variability probably through the effects on convective turbulence.

Urban developers and modelers can use this study to factor in the impact of local weather and microclimate on variation of temperature in densely populated cities. Such rules of thumb may help in anticipating power loads or designing cool cities.

Acknowledgements

This work was supported in part by NOAA grant NA11SEC481004 to the Cooperative Remote Sensing Science and Technology (CREST) Institute at the City College of New York, and by NOAA Regional Integrated Science Assessment (RISA) award #NA10OAR4310212 to the Consortium for Climate Risk in the Urban Northeast (CCRUN). The authors gratefully acknowledge data and imagery made available for fair use by NYC MetNet, the National Building Statistics Database, the US Geological Survey, and Google Earth.

References

Anisimov, O. A. (2001). Predicting patterns of near-surface air temperature using empirical data. Springer Link, 50(3), 297-315. Doi: 10.1023/a:1010658014439

Astrom, D. O., Bertil, F., & Joacim, R. (2011). Heat wave impact on morbidity and mortality in the elderly population: A review of recent studies. Maturitas, 69(2), 99-105. doi:10.1016/j.maturitas.2011.03.008

Bottyan, Z., & Unger, J. (2003). A multiple linear statistical model for estimating the mean maximum urban heat island. Theoretical and Applied Climatology,75 (3-4), 233-243. Doi: 10.1007/s00704-003-0735-7

Comrie, A. C. (2000). Mapping a wind–modified urban heat island in Tucson, Arizona (with Comments on Integrating Research and Undergraduate Learning).Bull. Amer. Meteor. Soc. Bulletin of the American Meteorological Society, 81(10), 2417-2431. Doi: 10.1175/1520-0477(2000)0812.3.co;2

Eliasson, I. (1996). Intra-urban nocturnal temperature differences: A multivariate approach. Climate Research Clim. Res., 7, 21-30. Doi: 10.3354/cr007021

Gladt, M., & Bednar, T. (2013). A new method for the calculation of the sky view factor for non-rectangular surroundings. 13th Conference of International Building Performance Simulation Association, 2839- 2844. Retrieved October 12, 2016, from http://www.ibpsa.org/proceedings/BS2013/p_995.pdf

Grimmond, S. (2007). Urbanization and global environmental change: Local effects of urban warming. The Geographical Journal Geographical J, 173(1), 83-88. doi:10.1111/j.1475-4959.2007.232_3.x

Ho, H. C., Knudby, A., Sirovyak, P., Xu, Y., Hodul, M., & Henderson, S. B. (2014). Mapping maximum urban air temperature on hot summer days. Remote Sensing of Environment, 154, 38-45. doi:10.1016/j.rse.2014.08.012

Katsouyanni, K., Trichopoulos, D., Zavitsanos, X., & Touloumi, G. (1988). The 1987 Athens heatwave. The Lancet, 332(8610), 573. Doi:10.1016/s0140-6736(88)92699-2

Karl, T. R., Diaz, H. F., & Kukla, G. (1988). Urbanization: its detection and effect in the United States climate record. Journal of Climate, 1(11), 1099-1123. Doi:10.1175/1520-0442(1988)0012.0.co;2

Karimi, M., Nazari, R., Vant-Hull, B., & Khanbilvardi, R. (2015). Urban heat island assessment with temperature maps using high resolution datasets measured at street level, The International Journal of the Constructed Environment, ISSN: 2154-8587, 1-15

Kenward, A., Yawitz, D., Sanford, T., & Wang, R. (2014). Summer in the city, hot and getting hotter. Climate Central 1-29.

Kinney, P. L., Sheffield, P. E., & Weinberger, K. R. (2013). Climate, air quality, and allergy: Emerging methods for detecting linkages. Global Climate Change and Public Health, 121-136. Doi:10.1007/978-1-4614-8417-2-7

MacKinnon, D.P., Krull, J.L., & Lockwood, C.M. (2000). Equivalence of the mediation, confounding and suppression effect. Prev Sci 1: 173. doi:10.1023/A:1026595011371

Meir, T., Orton, P., Pullen, J., Holt, T., Thompson, W., & Arend, M. (2013) Forecasting the New York City urban heat island and sea breeze during extreme heat events. Weather and Forecasting, doi: http://dx.doi.org/10.1175/WAF-D-13-00012.1

Montavez, J., Rodriguez, A., & Jimenez, J. (1999). A study of the urban heat island of Granada. International Journal of Climatology, 20(899), 911th ser., 899-911. Retrieved June 13, 2016, from http://hera.ugr.es/doi/15001647.pdf

Oke, T. R. (1982). The energetic basis of the urban heat island. Q.J Royal Met. Soc. Quarterly Journal of the Royal Meteorological Society, 108 (455), 1-24. Doi:10.1002/qj.49710845502

Robine, J., Cheung, S. L., Roy, S. L., Oyen, H. V., Griffiths, C., Michel, J., & Herrmann, F. R. (2008). Death toll exceeded 70 000 in Europe during the summer of 2003. Comptes Rendus Biologies, 331(2), 171-178. Doi:10.1016/j.crvi.2007.12.001

Semenza, J. C., Rubin, C. H., Falter, K. H., Selanikio, J. D., Flanders, W. D., Howe, H. L., & Wilhelm, J. L. (1996). Heat-related deaths during the July 1995 heat wave in Chicago. New England Journal of Medicine 335(2), 84-90. Doi: 10.1056/nejm199607113350203

U.S. Environmental Protection Agency. Climate change indicators in the United States- Heat related deaths (2014). http://www.coolrooftoolkit.org/knowledgebase/climate-change-indicators-in-the-united-states-heat-related-deaths/ Accessed July 2015

Vant-Hull, B., Karimi, M., Sossa, A., Wisanto, J., Nazari, R., & Khanbilvardi, R. (2014). Fine structure in Manhattan's daytime urban heat island: A new dataset. JUEE Journal of Urban and Environmental Engineering, 8(1), 59-74. Doi:10.4090/juee.2014.v8n1.059074

Voogt, J.a., & Oke, T.R. (2003). Thermal remote sensing of urban climates. Remote Sensing of Environment 86.3: 370-384.

Zhao, L., Lee, X., Smith, R. B., & Oleson, K. (2014). Strong contributions of local background climate to urban heat islands. Nature, 511(7508), 216-219. Doi:10.1038/nature13462

Zhang, J., Wang, Y., & Li, Yan. (2006). A C++ program for retrieving land surface temperature from the data of Landsat TM/ETM+ band6. Elsevier, Computers and Geosciences 32, 1796-1805. https://www.ncbi.nlm.nih.gov/pmc/articles/PMC2819361/

MacKinnon, D.P., Krull, J.L., & Lockwood, C.M. (2000). Equivalence of the mediation, confounding and suppression effect. Prev Sci 1: 173. doi:10.1023/A:1026595011371